J|A|C|S
ARTICLES
Published on Web 05/06/2006

Synthesis of Butane-Like SiGe Hydrides: Enabling Precursors for CVD of Ge-Rich Semiconductors

Andrew V. G. Chizmeshya,[§] Cole J. Ritter,[†] Changwu Hu,[‡] Jesse B. Tice,[†] John Tolle,[†] Ronald A. Nieman,[†] Ignatius S. T. Tsong,[‡] and John Kouvetakis*[,†]

Contribution from the Department of Chemistry and Biochemistry, Department of Physics and Astronomy, and Center for Solid State Science, Arizona State University, Tempe, Arizona, 85287

Received January 19, 2006; E-mail: jkouvetakis@asu.edu

Abstract: The synthesis of butane-like $(GeH_3)_2(SiH_2)_2$ (**1**), $(GeH_3)_2SiH(SiH_3)$ (**2**), and $(GeH_3)_2(SiH_2GeH_2)$ (**3**) Si−Ge hydrides with applications in low-temperature synthesis of Ge-rich $Si_{1-x}Ge_x$ optoelectronic alloys has been demonstrated. The compositional, vibrational, structural, and thermochemical properties of these compounds were studied by FTIR, multinuclear NMR, mass spectrometry, Rutherford backscattering, and density functional theory (DFT) simulations. The analyses indicate that the linear $(GeH_3)_2(SiH_2)_2$ (**1**) and $(GeH_3)_2(SiH_2GeH_2)$ (**3**) compounds exist as a mixture of the classic normal (*n*) and gauche (*g*) conformational isomers which do not seem to interconvert at 22 °C. The conformational proportions in the samples were determined using a new fitting procedure, which combines calculated molecular spectra to reproduce those observed by varying the global intensity, frequency scale, and admixture coefficients of the individual conformers. The $(GeH_3)_2(SiH_2)_2$ (**1**) species was then utilized to fabricate $Si_{0.50}Ge_{0.50}$ semiconductor alloys reflecting exactly the Si/Ge content of the precursor. Device quality layers were grown via gas source MBE directly on Si(100) at unprecedented low temperatures 350−450 °C and display homogeneous compositional and strain profiles, low threading dislocation densities, and atomically planar surfaces. Low energy electron microscopy (LEEM) analysis has demonstrated that the precursor is highly reactive on Si(100) surfaces, with H_2 desorption kinetics comparable to those of Ge_2H_6, despite the presence of strong Si−H bonds in the molecular structure.

Introduction

Heteroepitaxial $Ge_{1-x}Si_x$ layers on Si(100) with high Ge contents (above 50 at. %) are of interest due to many applications in key technologies such as solar cells, MEMS, quantum cascade lasers, and Si-based photonics[1,2] including high-speed modulators and photodetectors.[3] However, these materials are much less developed despite this high impact potential in IR optical devices. In addition, they serve as virtual substrates for growth of high mobility, strained Si and Ge device channels, and are also considered as a potential pathway to monolithic integration of III−V based devices with Si technologies.[4,5] The best current route to these materials is complicated and fraught with difficulties, requiring both high-temperature growth of thick (>10 μm) compositionally graded films and a chemical-mechanical planarization step to relieve the misfit strain between the $Ge_{1-x}Si_x$ epilayer and Si substrate and produce a flat surface.[6]

To circumvent these difficulties we have recently developed a new chemical vapor deposition (CVD) heteroepitaxy route to produce device quality strain-relieved Ge-rich films on Si without the need for graded compositions.[7,8] Our strategy involves depositions of single source hydride precursors with direct Si−Ge bonds such as the $(H_3Ge)_xSiH_{4-x}$ ($x = 1-4$) family of compounds. These are routinely synthesized with semiconductor grade purity via straightforward methodologies utilizing commercially available starting materials.[7] Their physical and chemical properties such as high volatility and facile reactivity make them particularly useful as reagents in low-temperature film growth by CVD and gas source molecular beam epitaxy (GSMBE). Our initial growth experiments have yielded single-crystal films with compositions $Si_{0.50}Ge_{0.50}$, $Si_{0.33}Ge_{0.67}$, $Si_{0.25}Ge_{0.75}$, and $Si_{0.20}Ge_{0.80}$, precisely matching those of the corresponding precursors SiH_3GeH_3, $(H_3Ge)_2SiH_2$, $(H_3Ge)_3SiH$, and $(H_3Ge)_4Si$.[8] Our results demonstrate that exact control of the composition, structure, and strain at the atomic level can be achieved via incorporation of the *entire* Si−Ge framework of the precursors into the film. The resulting films are of much higher quality than those previously reported using conventional

[†] Department of Chemistry and Biochemistry.
[‡] Department of Physics and Astronomy.
[§] Center for Solid State Science.

(1) Mooney, P. M.; Chu, J. O. *Annu. Rev. Mater. Sci.* **2000**, *30*, 335.
(2) Tromp, R. M.; Ross, F. M. *Annu. Rev. Mater. Sci.* **2000**, *30*, 431.
(3) Kuo, Y.-H.; Kyu, Y.; Ge, Y.; Ren, S.; Roth, J. E.; Kamins, T. I.; Miller, D. A. B.; Harris, J. S. *Nature* **2005**, *437*, 1334.
(4) Lee, M. L.; Pitera, A. J.; Fitzgerald, E. A. *J. Vac. Sci. Technol.* **2004**, *B 22* (*1*), 158.
(5) Kasper, E.; Heim, S. *Appl. Surf. Sci.* **2004**, *224*, 3.
(6) Currie, M. T.; Samavedam, S. B.; Langdo, T. A.; Leitz, C. W.; Fitzgerald, E. A. *Appl. Phys. Lett.* **1998**, *72* (*14*), 1718.
(7) Ritter, C. J.; Hu, C.; Chizmeshya, A. V. G.; Tolle, J.; Klewer, D.; Tsong, I. S. T.; Kouvetakis, J. *J. Am. Chem. Soc.* **2005**, *127* (27), 9855−9864.
(8) Hu, C.-W.; Menendez, J.; Tsong, I. S. T.; Tolle, J.; Chizmeshya, A. V. G.; Ritter, Cole; Kouvetakis, J. *Applied Physics Letters* **2005**, *87* (18), 181903/1−3.

sources and grow at much lower temperatures that are compatible with CMOS technology.

Within this compositional range the $Si_{0.50}Ge_{0.50}$ semiconductor system is of particular importance because it possesses the ideal lattice dimensions to integrate fully strained Si channels exhibiting high electron mobilities into metal oxide silicon field effect transistors (MOSFETS). Thus these materials are ideally suited for immediate technological applications in high-speed devices. However, in our experiments we have observed that stoichiometric $Si_{0.50}Ge_{0.50}$, with the required device quality properties (surface planarity, low defect densities), can only be grown near a maximum temperature of ~450 °C at a growth rate of only 0.2 nm/min which is too low to be practical for high throughput device fabrication. Negligible film growth was observed at lower temperatures via H_3GeSiH_3, while films with rough surfaces and high dislocation densities were obtained above ~500 °C due to the thermal mismatch with the substrate.

In our prior studies we have found that the growth rate increases significantly with increasing molecular weight in the H_3GeSiH_3, $(H_3Ge)_2SiH_2$, $(H_3Ge)_3SiH$, and $(H_3Ge)_4Si$ sequence of precursors.[7] The larger masses limit the surface diffusion and increase the sticking coefficients leading to rapid growth of atomically smooth films with reduced defect densities and uniform atomic distributions. This indicates that new compounds with increased reactivities and larger molecular weights than H_3GeSiH_3 should provide significantly improved growth characteristics of the desired $Si_{0.50}Ge_{0.50}$ alloys.

In this study we synthesize and fully characterize the butane-like $(GeH_3)_2(SiH_2)_2$ (**1**) compound containing highly reactive $-H_2Si-SiH_2-$ functionalities (rather than SiH_3). The $H_2Si{=}SiH_2$ dimeric unit has been identified as the dominant reactive intermediate in high temperature CVD via decomposition of conventional Si-hydrides. These species lead to highly efficient growth of homoepitaxial Si.[9] Precursor **1** is specifically designed to incorporate these necessary $-H_2Si-SiH_2-$ building blocks and provide a new low-temperature route for development of a broad range of Si-containing materials. Here we demonstrate the utility of **1** to produce device quality $Si_{0.50}Ge_{0.50}$ alloys at unprecedented low temperatures of 350 °C. A 10-fold improvement in the growth rate (~2.0 nm/min) is achieved at 350 °C relative to growth (0.2 nm/min) at 450 °C via GeH_3SiH_3 leading to uniformly stressed or strain-relaxed thin films directly on Si with planar surfaces and remarkably reduced dislocation densities. En route to **1** we have produced the isobutane analogue $(GeH_3)_2SiH(SiH_3)$ (**2**) and have also isolated and fully characterized the Ge-rich derivative $(GeH_3)_2(SiH_2GeH_2)$ (**3**). The latter is a moderately volatile liquid, with potential applications in low-temperature synthesis of Ge-rich optoelectronic alloys.

Results and Discussion

The synthesis of the main product 1,2-digermyldisilane, $(H_3Ge)_2(SiH_2)_2$ (**1**), was accomplished via reactions of $KGeH_3$ with the nonafluorobutane-sulfonic and triflate substituted disilanes $(C_4F_9SO_3)_2(SiH_2)_2$ (**4**) and $(SO_3CF_3)_2(SiH_2)_2$ (**5**) as illustrated by eqs 1 and 2, respectively. The starting materials **4** and **5** were prepared via reactions of the corresponding sulfonic acids $HSO_3C_4F_9$ and HSO_3CF_3 with 1,2-(*p*-tolyl)$_2$-$(SiH_2)_2$ (eqs 3 and 4, respectively).

$$(SO_3C_4F_9)_2(SiH_2)_2 + 2KGeH_3 \rightarrow (H_3Ge)_2(SiH_2)_2 + 2KSO_3C_4F_9 \quad (1)$$

$$(SO_3CF_3)_2(SiH_2)_2 + 2KGeH_3 \rightarrow (H_3Ge)_2(SiH_2)_2 + 2KSO_3CF_3 \quad (2)$$

$$(p\text{-tolyl})_2(SiH_2)_2 + 2\,HSO_3C_4F_9 \rightarrow (SO_3C_4F_9)_2(SiH_2)_2 + 2(\text{toluene}) \quad (3)$$

$$(p\text{-tolyl})_2(SiH_2)_2 + 2\,HSO_3CF_3 \rightarrow (SO_3CF_3)_2(SiH_2)_2 + 2(\text{toluene}) \quad (4)$$

The route described by eq 1 produced pure, single-phase $(H_3Ge)_2(SiH_2)_2$ (**1**) as a colorless, pyrophoric liquid. Here the replacement of $-SO_3C_4F_9$ by GeH_3 occurs exclusively at the 1,2-substitution sites of $(SO_3C_4F_9)_2(SiH_2)_2$ (**4**), as expected. However, the route described by eq 2 yields a mixture of products including $(GeH_3)_2(SiH_2)_2$ (**1**), the isobutane analogue $(GeH_3)_2SiH(SiH_3)$ (**2**), and the Ge-rich derivative $(GeH_3)_2(SiH_2GeH_2)$ (**3**) depending on reaction conditions (Figure 1). Specifically, low-temperature ($T \leftarrow 10$ °C) reactions of $(SO_3CF_3)_2(SiH_2)_2$ (**5**) with $KGeH_3$ (eq 2) afforded predominately **1** and impurity levels of **3**. These species are separated by distillation, and the minor low volatility fraction (vapor pressure of ~1 Torr at 22 °C) was characterized by a variety of spectroscopic methods as the Ge-rich derivative **3** possessing a heteronuclear H_2SiGeH_2 core (Figure 1). In contrast to the low-temperature pathways, the reaction of $(SO_3CF_3)_2(SiH_2)_2$ (**5**) with $KGeH_3$ at $T \geq 22$ °C yields predominately combinations of the positional isomers **1** and **2** in varying proportions (a small amount of **3** is also produced, but this is readily separated form the bulk via fractional distillation from the **1** and **2** mixture). In this case the replacement of SO_3CF_3 by GeH_3 initially occurs at the 1-substitution site of $(SO_3CF_3)_2(SiH_2)_2$ (**5**) as expected. The second replacement could produce germyl disilane, $SiH_3SiH_2GeH_3$, and germylene (GeH_2) intermediates rather than the 1,2-digermyldisilane, $(H_3Ge)_2(SiH_2)_2$ (**1**). Insertion of GeH_2 into $SiH_3SiH_2GeH_3$ then may yield $(GeH_3)_2SiH(SiH_3)$ (**3**) as shown in eq 5. A similar insertion mechanism (discussed in detail in subsequent sections) has been observed in the photochemical generation of gas phase *i*-Si_4H_{10} from SiH_2 insertion into trisilane $SiH_3-SiH_2-SiH_3$ (eq 6):

$$-SiH_2-SiH_2-GeH_3 + GeH_3 \rightarrow \text{“}SiH_3-SiH_2-GeH_3 + GeH_2\text{”} \rightarrow (GeH_3)_2SiH(SiH_3) \quad (5)$$

$$SiH_3-SiH_2-SiH_3 + SiH_2 \rightarrow (SiH_3)_2SiH(SiH_3) \quad (6)$$

The synthesis of **5** is described by eq 4 and has been previously demonstrated elsewhere. Its $(p\text{-tolyl})_2(SiH_2)_2$ starting materials has been produced via coupling reactions of (*p*-tolyl)-SiH_2Cl with powdered lithium.[10] In the present work we adopt a more convenient, analogous approach using readily available sodium fragments as the coupling agent. Compound **5** is obtained as a highly reactive liquid, which is difficult to fully handle and purify. Consequently its reactions with $KGeH_3$ are complex and produce mixtures of products as described above.

(9) Nijhawan, S.; McMurry, P. H.; Swihart, M. T.; Suh, S.-M.; Girshick, S. L.; Campbell, J. E. Brockmann, S. A. *Aerosol Science* **2003**, *34*, 691–711.
(10) Soldner, M.; Schier, A.; Schmidbaur, H. *J. Organomet. Chem.* **1996**, *521*, 295.

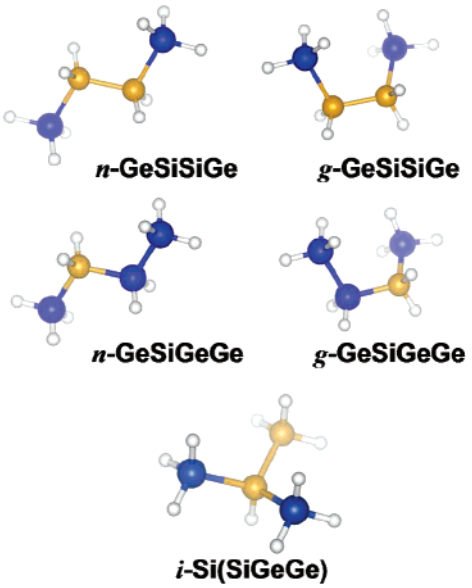

Figure 1. Molecular structures of the normal (*n*) and gauche (*g*) isomers for $(H_3Ge)_2(SiH_2)_2$ and $(GeH_3)_2(SiH_2GeH_2)$ [{*n*-GeSiSiGe, *g*-GeSiSiGe}/{*n*-GeSiGeGe, *g*-GeSiGeGe}, respectively] and of the positional isomer *i*-Si(SiGeGe) for $(GeH_3)_2SiH(SiH_3)$.

In contrast the newly prepared compound **4** is readily crystallized as a robust molecular solid that is completely isolated from the reaction byproducts and other contaminants, thereby leading to high purity $(H_3Ge)_2(SiH_2)_2$ in subsequent steps according to eq 1. The compositional, vibrational, and structural properties of the newly synthesized compounds **1**, **2**, **3**, and **4** are presented below.

$(H_3Ge)_2(SiH_2)_2$ (1): The $(H_3Ge)_2(SiH_2)_2$ (**1**) species is prepared as described by the reactions depicted in (eqs 1, 2) and was isolated and purified by fractional distillation (vapor pressure of ∼8−10 Torr at 22 °C). The FTIR, ^{29}Si NMR (proton-coupled), and mass spectra indicate a 1,2-digermyldisilane with a butane-like structure as shown in Figure 1. The IR spectrum shows the Si−H and Ge−H stretching modes at 2147 and 2073 cm^{-1}, respectively, and a set of absorption bands between 910 and 442 cm^{-1} corresponding to the bending modes of the molecule. These assignments are consistent with those made previously for the $(H_3Ge)_xSiH_{4-x}$ ($x = 1-4$) family of silyl germanes.[7] A more detailed interpretation of the full IR spectrum is obtained from quantum chemical calculations, and the data show fixed combinations between the butane-like normal and gauche conformers of (**1**) (see section below for details). The ^{1}H NMR spectra reveals a quartet at 3.29 ppm and a triplet at 3.11 ppm corresponding to the Si−H and Ge−H protons, respectively, which is consistent with a $H_3Ge-SiH_2-SiH_2-GeH_3$ molecular structure. This structure is further confirmed with 2D ^{1}H COSY and ^{1}H−^{29}Si HMQC NMR experiments. The 2D ^{1}H COSY spectrum showed cross-peaks that correlate to Si−H and Ge−H resonances at 3.29 and 3.11 ppm, respectively, indicating the H−Si−Ge−H connectivity. A proton-decoupled ^{1}H−^{29}Si HMQC spectrum showed that the H atoms at 3.29 ppm are directly attached to Si atoms at −105 ppm. The mass spectra revealed an isotopic envelope at 210−196 amu as the highest mass peak corresponding to the parent ion ($Si_2Ge_2H_x^+$). The associated fragmentation pattern is consistent with the proposed structure. The existence of **1** was further corroborated by Rutherford backscattering (RBS) analysis of monocrystalline films produced by single source MBE depositions of the compound at 350 °C (eq 7). The Si/Ge elemental content of the films was consistently 1:1 reflecting precisely the composition of the Si_2Ge_2 core of the molecule.

$$(H_3Ge)_2(SiH_2)_2\ (gas) \rightarrow 2SiGe\ (film) + 5H_2\ (gas) \quad (7)$$

$(GeH_3)_2SiH(SiH_3)$ (2): The isobutane-like structure of **2** was determined by ^{29}Si and ^{1}H NMR studies. The proton NMR resonances are present as a multiplet centered at 3.049 ppm due to −SiH and two doublets centered at 3.213 and 3.404 ppm corresponding to the $(-GeH_3)_2$ and $-SiH_3$ protons, respectively. The integrated peak intensity ratio of −SiH, $(-GeH_3)_2$, and $-SiH_3$ is 1:6:3, respectively, as expected. The peak intensities, the coupling patterns, and the position of the peaks in the spectrum collectively point to the isobutane-like structure in which an Si center is tetrahedrally bonded to two GeH_3 groups, one SiH_3 group, and a single H atom. This structure is further confirmed by 2D ^{1}H COSY and ^{1}H−^{29}Si HMQC NMR measurements. The 2D ^{1}H COSY spectrum showed cross-peaks that correlate to the central SiH, and terminal GeH_3 and SiH_3 resonances at 3.049, 3.213, and 3.404 ppm, respectively, indicating a $H_3Si-SiH-(GeH_3)_2$ connectivity, which is consistent with the proposed isobutane structure. A proton-decoupled ^{1}H−^{29}Si HMQC spectrum showed that the H atoms at 3.049 and 3.404 ppm are directly bonded to Si atoms at −121 and −93 ppm, respectively. The ^{29}Si chemical shift (−121 ppm, in C_6D_6) due to the central Si atom in this molecule is similar to those found for $SiH(GeH_3)_3$ (−113 ppm in $CDCl_3$) and $Si(GeH_3)_4$ (−128 ppm, in $CDCl_3$). A close correspondence is also found between the ^{29}Si chemical shift (−93 ppm) due to the terminal Si atom and those of the terminal SiH_3 groups (−92 ppm) for H_3GeH_3Si.

Gas-chromatography mass-spectrometry experiments (GCMS) of samples containing $(H_3Ge)_2(SiH_2)_2$ (**1**) and $(GeH_3)_2SiH(SiH_3)$ (**2**) indicated the presence of two major fractions that displayed slightly different retention times in the GC column, which is consistent with a mixture of **1** and **2** possessing slightly different boiling points. Furthermore, these fractions displayed essentially identical mass spectra. The highest mass peak is observed in the 210−196 amu range corresponding to the ($Si_2Ge_2H_x^+$) parent ions of **1** and **2**. Samples of the mixture were further characterized using IR spectroscopy. The spectra are essentially a simple admixture of the individual **1** and **2** components. The spectrum of **2** was theoretically determined since the compound could not be completely separated in pure form from **1** via our distillation method due to the similarity in their boiling points. The contributions of each compound in the experimental IR spectra were then determined using a fitting procedure involving both the observed and the calculated spectra.

$(GeH_3)_2(SiH_2GeH_2)$ (3): Compound (**3**) is a byproduct of the reaction described by eq 2. Its gas-phase IR spectrum shows the Si−H and Ge−H stretching bands centered at 2145 and 2073 cm^{-1}, respectively. The intensity of the Ge−H peak in the spectrum is significantly stronger than the Si−H due to the greater number of Ge−H bonds relative to Si−H bonds. The ^{1}H NMR spectra showed a set of two sextets at 3.30 and 3.03 ppm ensconcing two triplets at 3.23, 3.13 ppm. The integrated peak intensity ratios of the sextet-triplet−triplet-sextet sequence are 2:3:3:2. The integrated intensities the coupling patterns and the position of the peaks in the NMR spectrum collectively point

to a $H_3Ge-SiH_2-GeH_2-GeH_3$ molecular structure in which a central SiH_2GeH_2 core is bonded with two terminal GeH_3 moieties. In particular, the sextets at 3.30 and 3.03 ppm can be associated, respectively, with the SiH_2 and GeH_2 protons of the central $-SiH_2GeH_2-$ while the triplets at 3.23, 3.13 ppm correspond to terminal GeH_3 protons. The SiH_2 and GeH_2 NMR frequencies in this case correlate well with those in the previously reported $(H_3Ge)_2SiH_2$ and $GeH_3GeH_2SiH_3$ compounds.[7] The assignment of the sextet at 3.30 ppm to the SiH_2 protons was further corroborated by a $^1H-^{29}Si$ HMQC NMR spectrum, which indicates a direct coupling to a single ^{29}Si resonance found at −98.2 ppm. In addition, a 2D ^1H COSY NMR spectrum was used to unequivocally establish the specific ordering of the Ge−Si−Ge−Ge backbone constituents. Cross-peaks correlate an Si−H and three Ge−H resonances at 3.30, 3.23, 3.13, and 3.03 ppm. These correspond, respectively, to SiH_2, GeH_3 (terminal) connected to GeH_2, $Ge-H_3$ (terminal) connected to SiH_2, and GeH_2. The mass spectra showed an isotopic envelope at 256−238 amu as the highest mass peak corresponding to the parent ion ($SiGe_3H_x^+$) and a fragmentation pattern consistent with the molecular structure.

$(C_4F_9SO_3)_2(SiH_2)_2$ (4): Compound **4** is isolated at 95% yield as a colorless, pyrophoric solid with a melting point of 68 °C. It is readily soluble in ethers, $CHCl_3$, and CH_2Cl_2 and slightly soluble in toluene. The ^1H NMR spectrum showed a singlet centered at 5.08 ppm (δ Si−H) due to SiH_2 and ^{29}Si satellite peaks. These exhibit a triplet of triplets with a one-bond Si−H coupling of 272 Hz and a H−H three-bond coupling of 3.6 Hz. This indicates the presence of a second SiH_2 group consistent with the $-SiH_2SiH_2-$ core. Furthermore, a proton decoupled $^1H-^{29}Si$ HMQC showed that the proton resonance at 5.08 ppm is directly attached to a Si atom at −30.1 ppm. These values are consistent with those observed for the triflate analogue $(SO_3CF_3)_2(SiH_2)_2$ (**5**).[10] Compound **4** was further characterized by FTIR, mass spectrometry, and C, H, F elemental analysis, and the data are fully consistent with the proposed structure (see Experimental Section).

Ab Initio Simulations of Molecular Properties

Structural and Thermochemical Properties: To corroborate the identification of $(GeH_3)_2(SiH_2)_2$, $(GeH_3)_2SiH(SiH_3)$, and $(GeH_3)_2(SiH_2GeH_2)$ described above we simulated the structural, energetic, and vibrational trends of these compounds. In prior studies[7] we demonstrated that B3LYP hybrid density functional theory (DFT) simulations provide an excellent account of the ground-state structural, thermochemical, and vibrational properties of the $(H_3Ge)_xSiH_{4-x}$ family of molecular hydrides. In particular use of the 6-311G++(2d,2p) basis set yielded small typical bond length and frequency discrepancies (on the order of 0.4% and 1.4%, respectively). Accordingly, our first attempt at reconciling the observed IR spectra with those calculated was based on the same procedure and on the assumption that the fundamental structures are *n*-butane-like. Although this approach provided a close match to most of the main spectral features observed, several strong low-frequency features remained unaccounted for in the calculated IR pattern. In view of the prior success of the B3LYP approach we concluded that *n*-butane-like molecular structures alone could not account for the spectrum of the synthesized compounds. We therefore expanded our calculations to include the gauche conformational isomers in which a terminal GeH_3 group is rotated out of the Ge−Si−Si−Ge (or Ge−Si−Ge−Ge) skeletal plane, as well as the isobutane-like positional isomer *i*-Si(SiGeGe) (Figure 1). These isomers are completely analogous to those previously reported in tetrasilane and related molecules, and in subsequent discussion we simply refer to them as *n*-GeSiSiGe, *g*-GeSiSiGe, *n*-GeSiGeGe and *g*-GeSiGeGe, and *i*-Si(SiGeGe), as shown in Figure 1. Our results indicate that the observed spectra of both the synthesized compounds are completely accounted for by a admixture of the *n*-, *g*-, and *i*-type conformations.

Initial basis set convergence tests showed that a full resolution of differences in the calculated properties of the conformational/positional isomers requires an even more stringent treatment than that used in the prior studies on $(H_3Ge)_xSiH_{4-x}$ hydrides, particularly with regards to calculated vibrational properties. Accordingly all of the calculations described in the present work were carried out at the B3LYP/6-311G++(3df,2pd) level as implemented in the Gaussian03 code.[11]

The results of the structural optimizations, obtained using "tight" convergence criteria, are presented in Table 1. The table lists the bond length, bond angle, and bond torsion data for *n*-GeSiSiGe, *g*-GeSiSiGe, *n*-GeSiGeGe, *g*-GeSiGeGe, and *i*-Si(SiGeGe). In all molecules, the skeletal structure exhibits typical Si−Si and Si−Ge bonds with the gauche conformations exhibiting slightly (0.002 Å) longer/shorter Si−Si/Si−Ge bonds than their linear counterparts. In the isobutane-like isomer *i*-Si(SiGeGe) the Si−Si bond lengths (2.351 Å) are found to be intermediate to those in the other isomers, while the Si−Ge bond is dilated to a value of 2.400 Å. All the Si−Si values, 2.350−2.352 Å, correspond closely (∼0.1%) to that found in bulk silicon $a\sqrt{3}/4 = 2.352$ Å where a (5.431 Å) is the lattice constant of crystalline Si in the diamond structure. The Ge−Ge value found in *n*-GeSiGeGe and *g*-GeSiGeGe, 2.446 Å, is also close to that of bulk germanium (2.449 Å). The heteronuclear skeletal Si−Ge bond lengths exhibit a distribution in the range 2.396−2.400 Å and represent an average of the Si−Si and Ge−Ge values (2.399 Å).

The Si−H and Ge−H bond lengths occur exclusively as central SiH_2 moieties and terminal GeH_3 groups in the *n*- and *g*-GeSiSiGe isomers, with values of 1.486 Å and 1.539 Å, respectively. In the corresponding GeSiGeGe isomers the Si−H bonds associated with the SiH_2 moiety has essentially the same value, 1.485 Å, while the GeH_2 moiety exhibits a slightly longer Ge−H bond (1.542−1.548 Å) than that in a GeH_3 terminal group, as expected. Due to its unique structure the *i*-Si(SiGeGe) isomer possesses both terminal SiH_3 and GeH_3 groups and a single SiH moiety. Here the Ge−H bond lengths associated with the terminal GeH_3 groups have the same value (1.539 Å) as that in GeH_3 groups of other isomers, while the corresponding terminal group $Si-H_3$ bond lengths are slightly contracted (1.483 Å). The longest Si−H bond length is associated with the central SiH moiety and has a value of 1.488 Å. Collectively, these bond length trends are consistent with those found previously in the heaviest members of the $(H_3Ge)_xSiH_{4-x}$ ($x = 3, 4$) family of molecules.

The data presented in Table 1 also shows that the intermetallic skeletal bond angles, as well as those involving hydrogen−metal bonds, are essentially unchanged between all isomers studied. The only exception is found in the H−Ge−Si

(11) Frisch, M. J. et al. *Gaussian 03*, revision B.04; Gaussin Inc.; 2003.

Table 1. Calculated Thermochemical (300 K) and Structural Properties of the Conformational Isomer Pairs {*n*-GeSiSiGe, *g*-GeSiSiGe}, {*n*-GeSiGeGe, *g*-GeSiGeGe} and positional isomer *i*-Si(SiGeGe)[a]

	n-GeSiSiGe	*g*-GeSiSiGe	*i*-Si(SiGeGe)	*n*-GeSiGeGe	*g*-GeSiGeGe
			Bond Lengths		
Si−Si	2.350	2.352			2.351
Si−Ge	2.398	2.397	2.400	2.398	2.396, 2.400
Ge−Ge				2.446	2.446
Si−H	1.485	1.486	1.488, 1.483	1.485	1.485
Ge−H	1.539	1.538	1.539	1.548, 1.542	1.548, 1.542
			Bond Angles		
Ge−Si−Ge			110.7	112.7	112.8
Si−Ge−Ge				112.8	113.4
Ge−Si−Si	112.6	112.8	111.2		
H−Si−H	107.7	107.7	108.6	107.7	107.8
H−Ge−H	108.3	108.2	108.3		
H−Si−Ge	108.9	108.8	107.7	109.0, 109.2	109.0
H−Ge−Si	110.5, 110.5, 111.0	110.7		109.5, 110.5, 111.1	109.3, 110.7
H−Si−Si			108.4		
			Bond Torsions		
Ge−Si−Si−Ge	180.0	66.0	-33.1		
Ge−Si−Ge−Ge				180.0	64.1
H−Ge−Ge−H				58.2, 62.0, 178.4	58.4, 61.7, 178.5
H−Ge−Si−H	58.6, 61.5, 178.8	58.5, 61.9, 178.9	53.1, 72.6, 179.7	58.8, 61.4, 179.0	59.9, 60.1, 179.8
H−Ge−Si−Ge			57.6, 62.2, 177.8	59.8, 59.8, 180.0	58.7, 61.2, 178.8
H−Si−Ge−Ge			30.2	(58.6	57.0, 174.5
H−Ge−Si−Si	58.6, 61.5, 180.0	59.5, 60.4, 179.7	58.2, 61.8, 178.3		
			Energetics		
E_0	−4739.094 740	−4739.093 652	−4739.094 943	−6526.593 697	−6526.593 140
$E_0 + E_{ZPE}$	−4739.013 922	−4739.013 009	−4739.014 382	−6526.514 649	−6526.513 945
$E_0 + E_{tot}$	−4739.003 483	−4739.002 561	−4739.003 703	−6526.503 627	−6526.503 131
$E_0 + H_{corr}$	−4739.002 539	−4739.001 616	−4739.002 759	−6526.502 683	−6526.502 186
$E_0 + G_{corr}$	−4739.051 456	−4739.050 695	−4739.052 539	−6526.555 562	−6526.553 533

[a] The units for bond lengths, bond angles, and energies are angstroms, degrees, and hartree, respectively

bond angle distributions, which possess several values in the linear *n*-GeSiSiGe isomer and a unique value in all of the others. The Ge−Si−Si−Ge torsion angle in the linear molecules is 180°, indicating that the metal atoms are confined to a common plane, while the gauche conformations exhibit torsion angles of 66° and 64° in Ge−Si−Si−Ge and Ge−Si−Ge−Ge, respectively. It is also evident from the data that the intermetallic and metal−hydrogen bond angles in the *i*-Si(SiGeGe) isomer are, on average, closer to ideal tetrahedral values than those predicted for the other conformational/positional isomers.

Table 1 also lists the thermochemical energies of the molecules, including the total ground-state electronic energy E_0, and its value corrected for zero-point energy correction (E_{ZPE}), thermal energy (E_{CORR}), enthalpy (H_{CORR}), and free energy (G_{CORR}) at 298 K. In the case of the $Ge_2Si_2H_{10}$ molecules our calculations indicate that the *i*-Si(SiGeGe) isomer is slightly favored at room temperature, with a free energy difference of 0.0008 Hartree or about 2.0 kJ/mol (note: k_BT @ 300 K ≈ 2.4 kJ/mol) relative to *n*-GeSiSiGe. The latter molecule's free energy is, in turn, more stable than that of *g*-GeSiSiGe by about 2.8 kJ/mol. For the GeSiGeGe compound the *n*-GeSiGeGe isomer free energy is lower than that of its gauche conformation by 0.0020 Hartree (5.3 kJ/mol).

Vibrational Spectra: To facilitate the interpretation of the observed FTIR spectra we calculated the vibrational frequencies and intensities of the conformational isomers *n*-GeSiSiGe and *g*-GeSiSiGe and positional isomer *i*-Si(SiGeGe) of the primary product, as well as those of the minor species *n*-GeSiGeGe and *g*-GeSiGeGe, using the B3LYP DFT functional at the B3LYP/6-311G++(3df,2pd) level. No symmetry was imposed in the calculation of the frequency spectra, and all molecules studied exhibited a positive definite spectrum of harmonic frequencies indicating that the ground state structures are dynamically stable.

$Ge_2Si_2H_{10}$ Molecules: Figure 2 shows plots of the calculated spectra of *n*-GeSiSiGe, *g*-GeSiSiGe, and *i*-Si(SiGeGe), convoluted with a Gaussian of width ∼20 cm^{-1} to simulate experimental broadening. Both the high- and low-frequency regions are shown. It should also be noted that frequency scaling typically employed to reconcile the slight frequency overestimates obtained using this level of theory has not been applied to the calculated spectra shown in these plots. The interpretation of the high-frequency spectral features (Figure 2) is straightforward: the lower frequency pairs of peaks designated n_6 and n_7 in *n*-GeSiSiGe (Figure 2d), g_{11} and g_{12} in *g*-GeSiSiGe (Figure 2e), and i_{11} and i_{12} in *i*-Si(SiGeGe) (Figure 2f) correspond to symmetric and antisymmetric Ge−H stretching vibrations, respectively. Similarly, the symmetric and antisymmetric Si−H stretching vibrations are designated n_8 and n_9 in *n*-GeSiSiGe (Figure 2d), g_{13} and g_{14} in *g*-GeSiSiGe (Figure 2e), and i_{14} and i_{15} in *i*-Si(SiGeGe) (Figure 2f), respectively. The calculated splitting (13−14 cm^{-1}) between the symmetric and antisymmetric bands (in either Si−H or Ge−H) is approximately the same in all isomers; however, all of these bands are systematically lower (∼4−5 cm^{-1}) in frequency in the gauche isomer. In addition to these features the high-frequency spectrum of the positional isomer *i*-Si(SiGeGe), shown in Figure 2f, also exhibits an isolated vibrational feature near 2177 cm^{-1} (designated by i_{13} in Figure 2f), which corresponds to the central Si−H stretching vibration.

The low-frequency nonskeletal vibrational structure, also

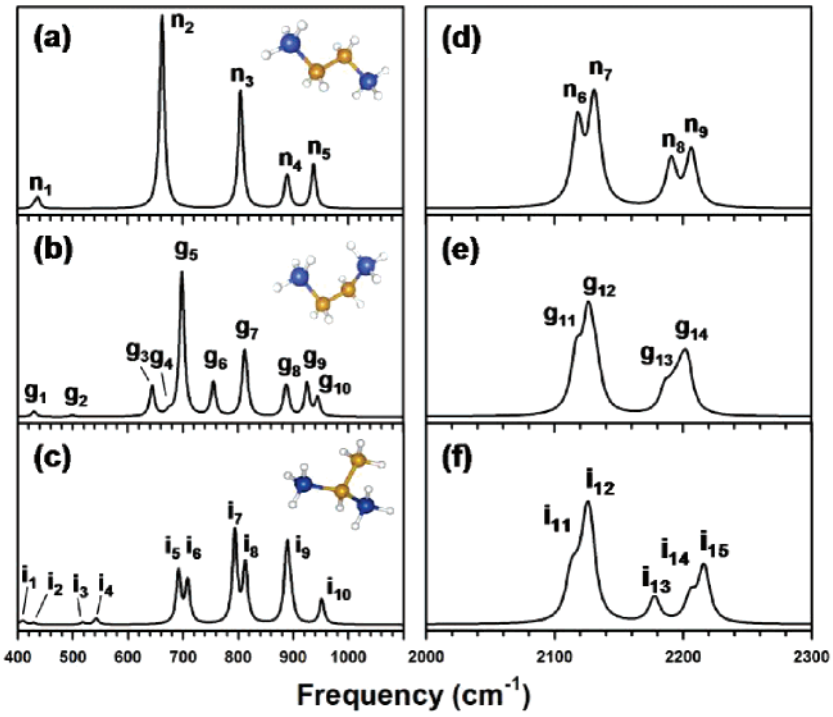

Figure 2. Calculated IR spectra of *n*-GeSiSiGe, *g*-GeSiSiGe, and *i*-Si(SiGeGe). The low- and high-frequency ranges are shown in panels {(a),(b),(c)} and {(d),(e),(f)}, respectively. Empirical frequency scaling has not been applied to the spectra shown here. Individual spectral features of the *n*-GeSiSiGe, *g*-GeSiSiGe, and *i*-Si(SiGeGe) molecules are labeled with "*n*", "*g*", and "*i*", respectively. Corresponding molecular structures are drawn as insets in the low-frequency plots.

shown in Figure 2, is considerably more complex and involves in- and out-of-plane, symmetric and antisymmetric Si−H/Ge−H wagging vibrations. The most striking difference between the spectra of *n*-GeSiSiGe and *g*-GeSiSiGe (parts a and b of Figure 2, respectively) is that four distinct features (n_2−n_5) of the linear isomer are effectively split in its gauche counterpart. For example, the strongest band in *n*-GeSiSiGe, n_2, corresponding to highly symmetric Si−H wagging vibrations parallel with the molecular backbone, is split into three bands denoted by g_3, g_5, and g_6 in the gauche isomer exhibiting very strong Si−H wagging parallel to the Si−Si bond. Among these, g_5 involves the least "crowded" protons in the molecule and accordingly exhibits the greatest intensity. The weak shoulder indicated by g_4 in the *g*-GeSiSiGe spectrum is the antisymmetric counterpart to mode g_5. Finally, the distinct feature near 925 cm^{-1} in the *n*-GeSiSiGe spectrum, n_5, corresponds to Si−H wagging vibrations perpendicular to the Si−Si axis involving symmetric H−Si−H bending motion. In the gauche isomer this band is split into symmetric and antisymmetric counterparts denoted by g_9 and g_{10}. Only a few bands appear to be common to both isomers. In particular features (n_1:g_1) near 430 cm^{-1} (asymmetrical wagging of the terminal Ge−H protons), (n_3:g_7) near 800 cm^{-1} (symmetrical terminal Ge−H wagging parallel to the Si−Si bond), and (n_4:g_8) near 876 cm^{-1} (terminal Ge−H wagging perpendicular to the Si−Ge bonds). The weak band designated g_2 in Figure 2b involves symmetrical terminal Ge−H wagging and has a silent counterpart in the *n*-GeSiSiGe molecule.

The low-frequency spectrum of *i*-Si(SiGeGe), shown in Figure 2c, has a slightly simpler structure due to the molecule's higher symmetry. The lowest frequency wagging modes found in the g-GeSiSiGe {g_1, g_2} are effectively split into asymmetrical pairs {i_1,i_2}, and {i_3,i_4}, respectively, in *i*-Si(SiGeGe). The dominant features near 800 cm^{-1} (i_7 and i_8) correspond to in-phase and anti-phase symmetrical Ge−H wags of the terminal GeH_3 groups while feature i_9 is the asymmetrical analogue to these vibrations. In the SiH_3 terminal group the Si−H wagging vibrations (i_{10}) occur at ∼951 cm^{-1}. Finally, features i_5 and i_6 are unique to the *i*-Si(SiGeGe) molecule and involve perpendicular Si−H wags of the SiH moiety.

$SiGe_3H_{10}$ Molecules: For the *n*- and *g*-$(GeH_3)_2(SiH_2GeH_2)$ isomers we corroborate the NMR characterization by directly comparing the observed IR spectrum with that calculated for a ∼1:3 mixture of *n*-GeSiGeGe and *g*-GeSiGeGe conformations (a detailed explanation is given in the following section). The calculated IR spectra for both the *n*- and *g*-isomer, convoluted with a Gaussian of width ∼20 cm^{-1} to simulate experimental broadening, are given in Figure 3. Both the high- and low-frequency regions are shown (no frequency scaling has been applied). Peaks in the simulated spectrum originating from *n*-GeSiGeGe or *g*-GeSiGeGe conformations are denoted by N_i and G_i, respectively.

The high-frequency Si−H stretching bands are similar to those found in the GeSiSiGe analogues, exhibiting a calculated splitting of 13−14 cm^{-1} between the symmetric and antisymmetric bands and a systematic overall ∼4−5 cm^{-1} shift to lower frequency in the gauche isomer. Here (N_{11}:G_{17}) and (N_{10}:G_{16}) correspond to asymmetric and symmetric Si−H stretches, respectively. However, a simple comparison for corresponding Ge−H stretching vibrations for these isomers is vitiated by the lower symmetry of GeSiGeGe isomers. For example the asymmetrical Ge−H stretch (N_9) in *n*-GeSiGeGe is split into contributions G_{12}, G_{14}, and G_{15} in the gauche isomer while the symmetric Ge−H stretch, N_8 in the *n*-GeSiGeGe, is split into bands G_{11} and G_{13}.

In the low-frequency range of the spectrum we find a strong

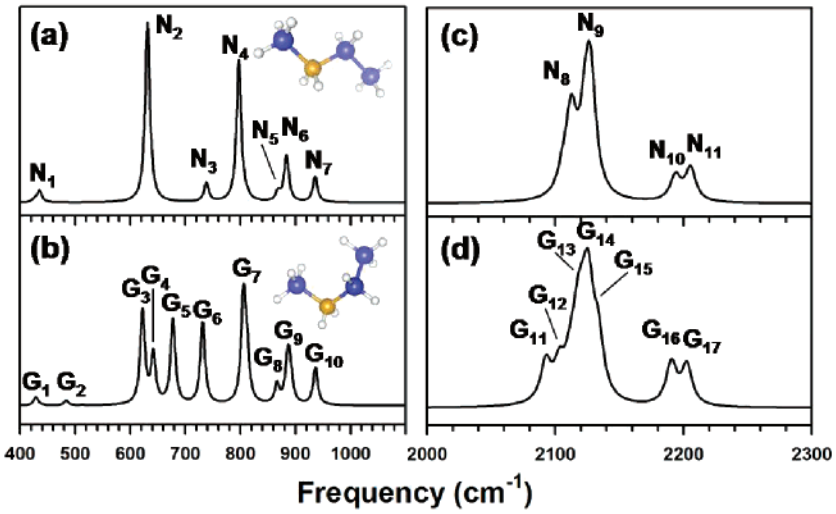

Figure 3. Calculated IR spectra of *n*-GeSiGeGe and *g*-GeSiGeGe. The low- and high-frequency ranges are shown in panels {(a),(b)} and {(c),(d)}, respectively. The spectral features of the *n*-GeSiGeGe and *g*-GeSiGeGe isomers are labeled "N" and "G", respectively. Empirical frequency scaling has not been applied to the spectra shown here. Corresponding molecular structures are drawn as insets in the low-frequency plots.

correspondence between mode assignments of the *n*- and *g*-isomers above 700 cm^{-1}. Specifically, the asymmetrical H−Si−H wagging vibrations N_3 in *n*-GeSiGeGe appears as G_6 in *g*-GeSiGeGe, with a frequency near 731 cm^{-1}. As in our earlier discussion we designate such corresponding pairs between isomer conformations as (N_3:G_6). Intense Ge−H wagging vibrations (N_4:G_7) associated with terminal GeH_3 groups appear near 808 cm^{-1}. Similarly, H−Ge−H "scissor" modes at 866 cm^{-1} are designated as (N_5:G_8), while their H−Si−H counterparts (N_7:G_{10}) appear at 936 cm^{-1} (the frequency of the corresponding mode in the GeSiSiGe isomers was ∼925 cm^{-1}). The features denoted (N_6:G_9) consist of asymmetrical "scissor"-like vibrations associated with the terminal GeH_3 groups.

The most significant differences between the IR spectra of the n- and g- isomers are found below 700 cm^{-1}. The most intense spectral feature in *n*-GeSiGeGe (N_2) is associated with a highly symmetric wagging of the protons bound to the GeH_2 moiety parallel to the molecular backbone. In the gauche isomer this mode is split into three features denoted G_3, G_4, and G_5, corresponding to asymmetrical Ge−H wagging of combinations of individual protons in the GeH_2 moiety. Finally, the mode N_1 in the *n*-isomer, consisting of concerted symmetrical wagging of terminal GeH_3 protons at both ends of the molecule, is split into two modes G_1 and G_2 in the gauche isomer in which symmetrical wagging occurs independently in the two GeH_3 terminal groups.

Isomer Admixture Analysis: To estimate the molar concentration of the comformational and positional isomers in the observed spectra, we adopt an approach commonly employed in "multiphase" fitting of X-ray spectra, in which a normalized admixture of known pure-phase candidate spectra is fitted to an unknown observed spectrum of the combined molecules. Using the same procedures as those in our prior studies on Si−Ge hydrides we have calculated the spectra of 10 digermyldisilyl positional/conformational isomers (to be described elsewhere). These calculated spectra serve as a proxy for the unknown pure isomer candidate spectra normally supplied by experiment. A comparison of our calculated spectra with that of the synthesized compounds suggests the presence of simple admixtures of conformational {*n*-GeSiSiGe, *g*-GeSiSiGe} and positional {*i*-Si(SiGeGe), *g*-GeSiSiGe} isomers for the $Si_2Ge_2H_{10}$ family. To proceed with the analysis all of the required theoretical spectra (*n*-, *g*-, and *iso*-isomers, see Figure 2) are first calculated on a fine frequency grid (1 cm^{-1} spacing) and then partitioned into low-frequency (0−1600 cm^{-1}) and high-frequency (1600−2600 cm^{-1}) regions. We denote the low-frequency spectra of the {*n*-GeSiSiGe, *g*-GeSiSiGe} pair by $\{I_n(\omega), I_g(\omega)\}$ and those of {*i*-Si(SiGeGe), *g*-GeSiSiGe} by $\{I_i(\omega), I_g(\omega)\}$. The corresponding observed spectrum of the synthesized compound, $I_{exp}(\omega)$, produced on a discrete frequency grid $\{\omega_k\}$ by the spectrometer (resolution ∼ 2−3 cm^{-1}), is then used to construct an objective function (eq 8). For example, in the case of the {*n*-GeSiSiGe, *g*-GeSiSiGe} admixture:

$$O(\beta,\gamma,\eta) = \sum_k \{I_{exp}(\omega_k) - \beta[\gamma I_n(\eta\omega_k) + (1-\gamma) I_g(\eta\omega_k)]\}^2 \quad (8)$$

where γ is the normalized admixture of *n*- and *g*-spectra, β is the global amplitude of the theoretical spectrum and η is the common frequency scale factor applied to the theoretical spectra. An identical procedure is used to treat the {*i*-Si(SiGeGe), *g*-GeSiSiGe} combination. In all cases the theoretical spectra were evaluated at arbitrary frequencies using cubic splines, and a robust simplex method was used to minimize the objective function. For the {*n*-GeSiSiGe, *g*-GeSiSiGe} pair this yields a scale factor of $\eta = 0.984$ and an admixture of $\gamma = 0.392$ (i.e., ∼39% *n*-GeSiSiGe). This optimized scale factor is very similar to the value 0.989 used in previous studies of the $(H_3Ge)_xSiH_{4-x}$ hydrides[7] and Si_2H_6, Ge_2H_6 and H_3GeSiH_3 molecules[12] at this level of theory. As shown in Figure 4a the resulting low-frequency composite theoretical spectrum (ω < 1600 cm^{-1}), generated using this scale factor, agrees remarkably well with the observed one. To simulate the composite high-frequency spectrum for {*n*-GeSiSiGe, *g*-GeSiSiGe} we employ the admixture parameter derived from low-frequency behavior, $\gamma = 0.392$, and reduce the scale factor to $\eta' = (0.9909\eta) = 0.975$.

(12) Urban, J.; Schreiner, P. R.; Vacek, G.; Schleyer, P.; Huang, J. Q.; Leszczynski, J. *Chem. Phys. Lett.* **1997**, *264*, 441.

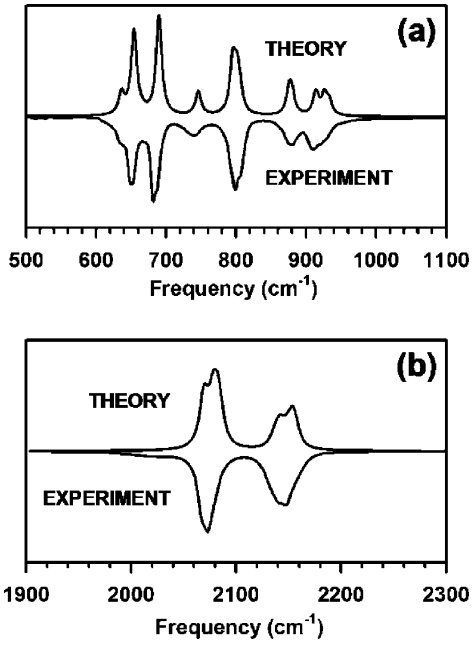

Figure 4. Comparison of an experimental spectrum of $(GeH_3)_2(SiH_2)_2$ (**1**) with a superposition of theoretical spectra for the {*n*-GeSiSiGe, *g*-GeSiSiGe} combination: (a) low-frequency region (500−1100 cm^{-1}) and (b) high-frequency Si−H/Ge−H region (1900−2300 cm^{-1}).

This low- to high-frequency scale factor ratio was previously found to yield an excellent account of the scaling behavior in related molecules.[12] Figure 4b demonstrates that the optimized parameters obtained using fits to the low-frequency spectra also faithfully and independently reproduce the high-frequency behavior, confirming the integrity of our procedure. Application of the foregoing low-frequency analysis to the positional isomeric combination {*i*-Si(SiGeGe), *g*-GeSiSiGe} yields $\eta = 0.985$ and $\gamma = 0.678$ (i.e., ∼68% *i*-Si(SiGeGe). The sample spectrum is compared with the calculated admixture in Figure 5, which indicates that the vibrational structure is largely accounted for using the admixture procedure.

The corresponding results for the GeSiGeGe compound are shown in Figure 6. A completely analogous fitting procedure to that above yields, in this case, an admixture parameter $\gamma = 0.235$ (i.e., 23.5% *n*-GeSiGeGe) indicating that the gauche conformation (*g*-GeSiGeGe) is dominant in the gas phase. As in the GeSiSiGe analysis, we find that fitting parameters obtained from the low-frequency spectrum (ω < 1600 cm^{-1}) yields an excellent account of the high-frequency stretching bands using the reduced frequency scale factor 0.975 (Figure 6b).

Remarks on Conformational and Isomeric Stability: We have observed that the proportions derived for the *n* and *g* conformational isomers do not change very much between different samples. To elucidate this observation we calculated the potential energy surface (PES) of the butane-like GeSiSiGe as a function of the Ge−Si−Si−Ge backbone torsion angle. The linear conformation corresponds a torsion angle of 180°, while the gauche modification occurs at ∼66° (see Table 1). For each fixed value of the torsion angle all remaining structural degrees of the freedom are optimized resulting in a "relaxed" PES. Figure 7 compares the torsional PES for butane (C_4H_{10}), tetrasilane (Si_4H_{10}), and GeSiSiGe ($Si_2Ge_2H_{10}$) at the DFT B3LYP/6-311G++(3df,2pd) and ab initio CCSD/LANL2DZ

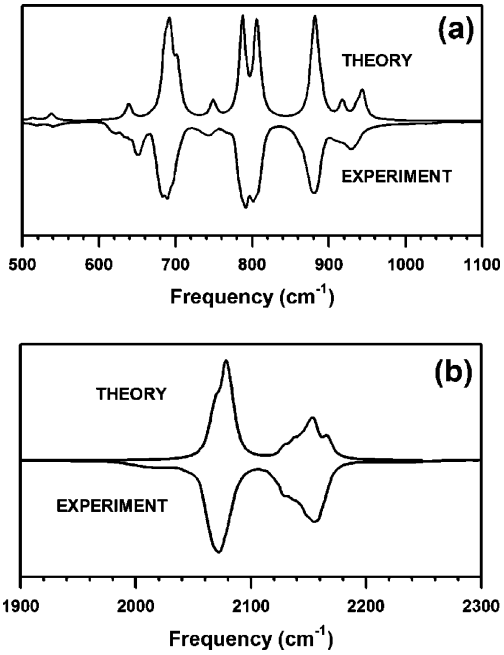

Figure 5. Comparison of an experimental spectrum of a $Si_2Ge_2H_{10}$ sample [containing a mixture of **1** and **2**] with a superposition of theoretical spectra for the {*i*-Si(SiGeGe), *g*-GeSiSiGe} combination: (a) low-frequency region and (b) high-frequency Si−H/Ge−H region. The theoretical spectra consist of an admixture of 68% *i*-Si(SiGeGe) and 32% *g*-GeSiSiGe.

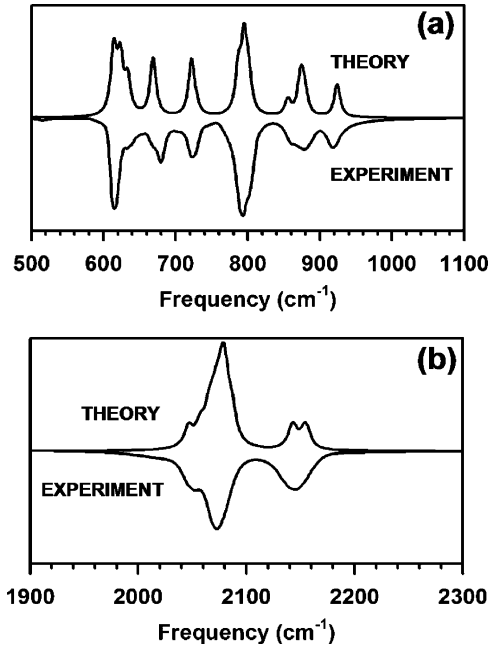

Figure 6. Comparison of an experimental spectrum of $(GeH_3)_2(SiH_2GeH_2)$ with a superposition of theoretical spectra for the {*n*-GeSiGeGe, *g*-GeSiGeGe} combination: (a) low-frequency region and (b) high-frequency Si−H/Ge−H region. The theoretical spectra consist of an admixture of 23% *n*-GeSiGeGe and 77% *g*-GeSiGeGe.

levels of theory. In all cases the value of the linear (or *trans*-) configuration is chosen as the reference energy. The figure shows that all three molecules exhibit very similar energy-torsion profile plots with a global minimum at 180°, a *n*−*g* barrier (E_{n-g}) at ∼120°, a local minimum at the gauche configuration (E_g) near 66° and a maximum value corresponding to the eclipse saddle point (E_e). Using the DFT B3LYP/6-311G++(3df,2pd) description we obtain $\Delta E_{n-g} = 0.942$, $\Delta E_g = 0.362$, and ΔE_e

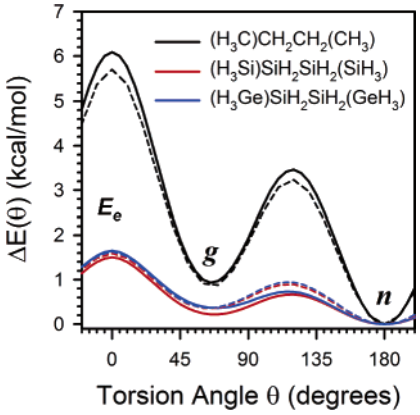

Figure 7. Relaxed potential energy surface as a function of the molecular backbone torsion angle for butane (black), tetrasilane (red), and GeSiSiGe (blue). Solid and dashed lines correspond to CCSD/LANL2DZ and B3LYP/6-311G++ (3df,2pd) calculations, respectively. The plots show that the gauche (*g*) GeSiSiGe is very slightly metastable compared to the linear (*n*) and that the *n*−*g* energy barrier is very small on a thermal energy scale consistent with the mixture of conformations observed in the IR spectra of the molecule.

= 1.628 kcal/mol for GeSiSiGe, while the corresponding tetrasilane values are 0.895, 0.360, and 1.591 kcal/mol, respectively. At this level of theory the conformational energy structures of GeSiSiGe and tetrasilane are essentially identical. This is not unexpected in view of their very similar bond characters. At the same level of description we find that the analogous PES for butane has the same qualitative shape as that of tetrasilane and GeSiSiGe but with significantly larger rotational barriers $\Delta E_{n-g} = 3.235$, $\Delta E_g = 0.884$, and $\Delta E_e = 5.713$ kcal/mol. This is likely due to the shorter/stronger C−C bonds within the carbon chain backbone, which lead to a concomitant increase in H repulsion. In contrast to butane the reduced proton repulsion in tetrasilane, GeSiSiGe, and related silane-germane compounds, due to longer Si−Si, Si−Ge, and Ge−Ge bonds, leads to small torsional barriers consistent with the facile low-temperature conformational interconversions observed experimentally.

We note that our B3LYP/6-311G++(3df,2pd) tetrasilane values for ΔE_{n-g} and ΔE_e are qualitatively different from those calculated by Albinsson et al.[13] at the MP2/6-31* level for the same molecule. In particular they predict a symmetric *n*−*g* barrier and nearly identical gauche and linear conformation energies ($\Delta E_{n-g} \approx 0.588$, $\Delta E_g \approx -0.04$, and $\Delta E_e \approx 1.236$ kcal/mol). Unfortunately, because the basis set levels and model chemistries in our two approaches both differ, the origin of this discrepancy is ambiguous. We therefore carried out a series of higher-level (CCSD/LANL2DZ) coupled cluster calculations for butane, tetrasilane, and GeSiSiGe. This allows comparison of all three molecules on the same footing. The results, shown as solid lines in Figure 7, are remarkably consistent with our B3LYP-based DFT calculations (dashed lines in the figure) and indicate that the linear (*n)* butane-like conformation is the ground-state structure, with a gauche value of $\Delta E_g \approx 0.2-0.4$ kcal/mol. Furthermore, the magnitude of the *barrier* connecting the gauche and linear conformations in GeSiSiGe is reduced to 0.36 kcal/mol (∼188 K) in the CCSD/LANL2DZ calculations.

It should be noted that the 68% proportion obtained for the positional *i*-Si(SiGeGe) isomer in the spectrum of {*i*-Si(SiGeGe), *g*-GeSiSiGe}, shown in Figure 5, is characteristic of *one* particular sample. Unlike the conformational isomers, which exhibited a fairly constant proportion between samples, the proportions of the positional isomers sensitively depend on the specific reaction conditions. This suggests that once the {*i*-Si(SiGeGe), *g*-GeSiSiGe} mixture has been isolated no interconversion between positional isomers occurs.

Chain cleavage and spontaneous isomerization are observed in the closely related tetrasilane Si_4H_{10} system during photochemical matrix isolation experiments producing trisilane (Si_3H_8) and silylene (SiH_2).[13] The formation *i*-Si_4H_{10} observed as a mixture with *n*-Si_4H_{10} is then believed to follow from SiH_2 insertion into the Si−H bonds of trisilane. As discussed in detail by Jasinski et al. this insertion reaction is one of the characteristic mechanisms in gas-phase polysilane chemistry, possessing a slight *negative* activation energy and a very high collisional efficiency.[14] We surmise that an analogous low energy germylene insertion reaction channel is present in our synthesis route (see eq 2) involving the triflate-substituted disilanes at $T > 22$ °C, leading to the condensation of *i*-Si(SiGeGe). One plausible mechanism could involve the replacement of $-SO_3CF_3$ by GeH_3 at the 1-substitution site of $(SO_3CF_3)_2(SiH_2)_2$ (**5**), followed by insertion of GeH_2 in the Si−H bonds of the central SiH_2 site in the $-SiH_2-SiH_2-GeH_3$ intermediate.

Deposition Studies

The deposition experiments were conducted on clean Si(100) substrates in an ultrahigh vacuum system equipped with a low energy electron microscope (LEEM) that allowed in situ real time observation of the growth process. The substrates were RCA prepared, and their surface was cleaned by repeated flashing at 1200 °C prior to growth. The $(H_3Ge)_2(SiH_2)_2$ gaseous precursor reacted on the Si surface via complete H_2 elimination at partial pressures in the range $10^{-5}-10^{-8}$ Torr. Initially, the reaction growth kinetics was investigated using LEEM, and the activation energy (E_{act}) of the compound with respect to H_2 desorption from the Si surface was measured. It is known that for conventional silanes and germanes the E_{act} is much lower on a Ge containing surface (including $Si_{1-x}Ge_x$) than on pristine Si. Thus, an accurate determination of E_{act} can only be obtained from measuring the growth rate of the first monolayer (which grows directly on pure Si) and not that of subsequent layers, which grow on Ge containing surfaces and have higher growth rates. In this regard LEEM is particularly unique because its dynamic imaging differentiates the Si(001)-(2 × 1) surface from the $Si_{1-x}Ge_x$ epilayer and thus provides unambiguous means for the correct determination of E_{act} on Si by measuring the growth rate of the first $Si_{1-x}Ge_x$ monolayer vs temperature.

For comparison the growth rates of Ge_2H_6 and H_3GeSiH_3 were also determined using the same method. For these and for $(H_3Ge)_2(SiH_2)_2$ the first monolayer took longer to complete on pristine Si than on subsequent monolayers. Figure 8 is a graph showing plots of the temperature dependence of the first layer growth rates. The activation energies were determined using the relation $R \approx \exp(-E_a/kT)$. The data are consistent with the first-order H_2 desorption kinetics and yield an E_{act} of 1.95, 1.66, and 1.42 eV, for H_3GeSiH_3, Ge_2H_6, and $(H_3Ge)_2(SiH_2)_2$, respectively. This indicates that the latter is not only more reactive than H_3GeSiH_3 but also more reactive than pure

(13) Albinsson, B.; Teramae, H.; Plitt, H. S.; Goss, L. M.; Schmidbaur, H.; Michl, J. *J. Phys. Chem.* **1996**, *100*, 8681.

(14) Jasinski, J. M.; Becerra, R.; Walsh, R. *Chem.* Rev. **1995**, *95*, 1203.

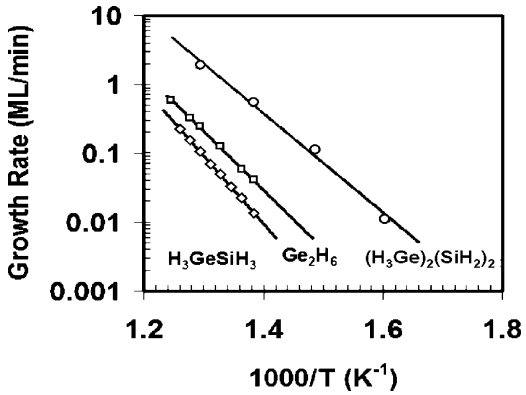

Figure 8. Temperature dependence of the first layer growth rates for thee precursors: H_3GeSiH_3, Ge_2H_6, and $(H_3Ge)_2(SiH)_2$ (**1**). The activation energies for these compounds are 1.95, 1.66, and 1.42 eV, respectively.

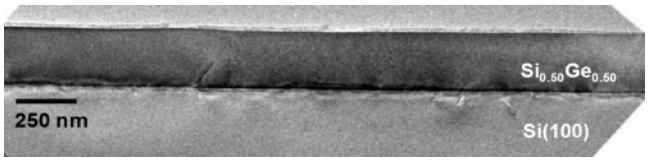

Figure 9. XTEM micrograph of a $Si_{0.50}Ge_{0.50}$ layer grown on Si(100) at 350 °C. No threading defects are observed within the field of view of ~2.5 μm, indicating a dislocation density of $<10^6/cm^2$.

Ge_2H_6 despite the presence of strong Si−H bonds in the molecular structure. Accordingly, it represents a unique high-reactivity species suitable for low temperature (300−400 °C) rapid growth of thick layers (100−500 nm) with stoichiometry $Si_{0.50}Ge_{0.50}$ reflecting that of the corresponding precursor. Below we describe the deposition procedure and key results regarding morphology, microstructure, composition, and strain for the films.

The synthesis of $Si_{0.5}Ge_{0.5}$ films was investigated in the 350−500 °C range via dehydrogenation of $(H_3Ge)_2(SiH_2)_2$. The highest temperature that yields planar layers is ~450 °C. The growth rate is ~4 nm/min and decreases to 2 nm/min at 350 °C. No appreciable growth was observed below 300 °C (1×10^{-5} Torr) due to the reduced reactivity of the compound. Thick films with rough surfaces and defective microstructures were produced at 500 °C with growth rates as high as 15 nm/min. The composition and heteroepitaxial character of the films were investigated by random and channeling Rutherford backscattering (RBS), which in all cases indicate a highly stoichiometric material aligned with the substrate. The ratio of the aligned versus the random peak heights (χ_{min}), which measures the degree of crystallinity, decreases from 15% at the interface to 6% at the surface indicating a dramatic reduction in dislocation density across the thickness of the film. This is confirmed by high resolution XTEM, which revealed commensurate SiGe/Si interfaces and perfectly monocrystalline layer microstructures. A survey of TEM samples showed no defects penetrating through the layers within a field of view of ~2.5 μm in the micrographs indicating an upper limit in the threading dislocation density of $\sim 10^6/cm^2$ (Figure 9). Most of the defects due to the lattice mismatch are concentrated near the interface region. In fact, a number of these appear to originate at the SiGe/Si interface and show a propensity to propagate downward into the substrate (Figure 10). Occasional edge dislocations spaced by ~150 nm are also observed in the vicinity of steps on the Si surface (Figure 10). These are parallel to the interface plane and may provide stress relief between the film and the substrate. The presence of edge dislocations is unusual since SiGe-based materials typically display (111)-threading dislocations and stacking faults. X-ray diffraction (XRD) revealed highly aligned layers with mosaics spreads as low as 0.1° and relatively strain free microstructures. Raman scattering experiments conducted with several Ar+ laser lines revealed a high degree of vertical uniformity in concentration and strain.[8] The Raman analysis indicated that the composition agrees well with the RBS value and that the strain relaxation is 75% and 95% for films with thicknesses of 200 and 500 nm, respectively, which are similar to those obtained by XRD.

Atomic force microscopy (AFM) studies show that films with thickness of 50 and 750 nm display RMS values of 0.5 and 1.5 nm, respectively, for 10×10 μm^2 areas, indicating highly planar surfaces for samples grown at $T < 450$ °C as shown in Figure 11b. For layers grown at $T > 450$ °C the AFM images [Figure 11a] show a classic "crosshatched" surface pattern caused by misfit dislocations produced during strain relaxation. It has been shown that both defect-induced interface and bulk alloy scattering considerably reduce the electron mobililties in these samples and degrade the device performance.[15] Nevertheless conventional CVD at ultralow pressure is known to produce $Si_{1-x}Ge_x$ materials with significantly lower crosshatching patterns leading to higher quality electrical properties.[15] In our experiments the high reactivity and low surface mobility of the $(H_3Ge)_2(SiH_2)_2$ compound permit low growth temperature and promote high growth rates at pressures of $\sim 10^{-5}$ Torr leading to high quality films devoid of crosshatched surface morphologies. It is interesting to note that the surface planarity of our samples is remarkably robust thermally. XRD scans and RBS (aligned) spectra of samples annealed between 450 and 750 °C were essentially identical before and after annealing. This result also confirms full relaxation in the as-grown layers at $T < 450$ °C.

Our deposition results indicate that we can obtain precise control of surface morphology composition (at the nanoscale) and defect free microstructure, all of which ultimately determine the physical properties and performance of the target materials. Figure 12 illustrates schematically the nucleation and growth of stoichiometric $Si_{0.50}Ge_{0.50}$ derived from successive reactions of individual *n*-GeSiSiGe molecules. In the process depicted here the precise elemental composition *and structure* of each molecular core are incorporated intact into the film at every step, resulting in a completely random distribution of Si and Ge atoms within each (001) monolayer of cubic symmetry. It should be noted that the apparent horizontal bias in the first few steps of the island construction in Figure 12 (steps 1−3) is associated with the exclusive use of *n*-GeSiSiGe units. In the actual low-temperature growth process the availability of gauche conformers promotes a more realistic and homogeneous nucleation of the (001) cluster geometries. Nevertheless, the incorporation of the massive Si_2Ge_2 molecular units leads to low surface diffusion and thus highly uniform compositional and strain profiles at the atomic level. This is in contrast to the *uncontrolled (diffusion-driven) elemental mixing* associated with conventional processes such as CVD of low order silanes and

(15) Cullis, A. G.; Robbins, D. J.; Pidduck A. J.; Smith, P. W. *J. Cryst. Growth* **1992**, *123*, 333.

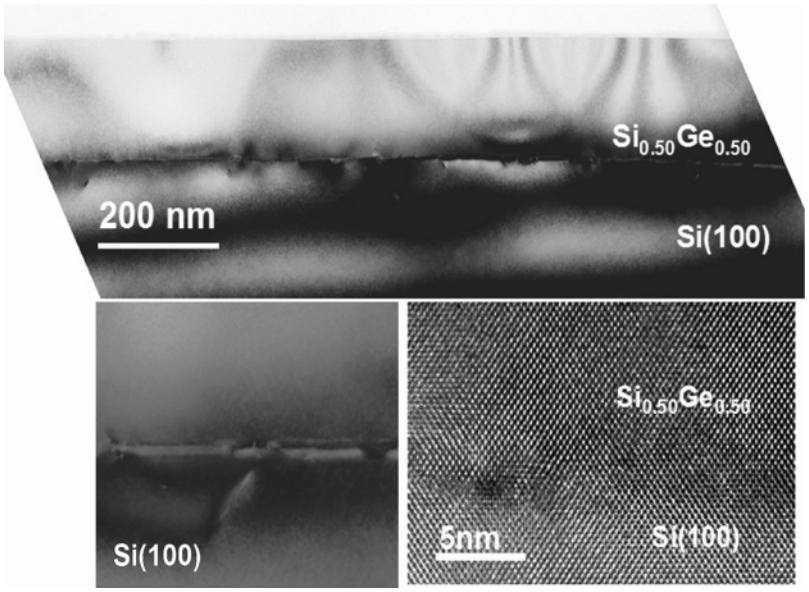

Figure 10. Diffraction contrast, high resolution XTEM micrographs of a $Si_{0.50}Ge_{0.50}$ layer grown on Si(100) at 400 °C. The film is nearly strain-free (~85%) and displays an atomically smooth surface free of threading defects (top). The mismatch with Si(100) is accommodated by dislocations located at the interface (bottom right). Defects originating at the interface show the propensity to penetrate downward into the substrate (bottom left).

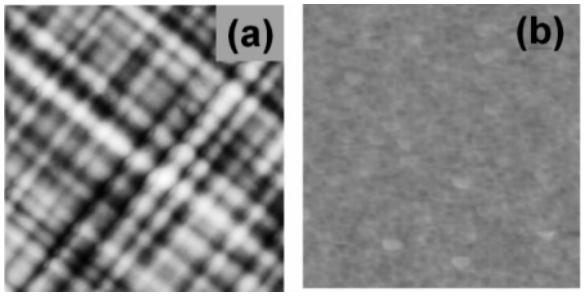

Figure 11. (a) AFM image of $Si_{0.50}Ge_{0.50}$ on Si(100) showing the crosshatch pattern morphology with an RMS roughness of 2.3 nm. (b) AFM image of a strain-relaxed and completely planar film with an RMS roughness of 0.5 nm.

germanes (SiH_4, Si_2H_6, GeH_4, and Ge_2H_6) or MBE of solid Si and Ge sources.

Conclusion

We have demonstrated the synthesis of the butane-like compounds with molecular formulas $(GeH_3)_2(SiH_2)_2$ (**1**), $(GeH_3)_2SiH(SiH_3)$ (**2**), and $(GeH_3)_2(SiH_2GeH_2)$ (**3**) and their conformational isomers. Detailed characterization of the products was conducted via a range of spectroscopic and analytical methods including quantum chemical simulations. A new fitting procedure was developed, based on the admixture of normal and gauche calculated spectra, to obtain the proportions of the individual conformers in the product sample at 22 °C. Controlled depositions of **1** have produced stoichiometric SiGe films possessing the desired properties for semiconductor applications including perfectly crystalline and epitaxial microstructures, smooth morphologies, and uniformly strain-relaxed states. Unique practical advantages associated with this low temperature (~350−450 °C) rapid growth include (i) short deposition times compatible with preprocessed Si wafers, (ii) selective growth for application in high frequency devices, and (iii) negligible mass segregation of dopants, which is particularly critical for thin layers. Finally we have found that these compounds are remarkably stable over extended periods of time, with no evidence of decomposition, and thus represent viable molecular sources for potential industrial applications.

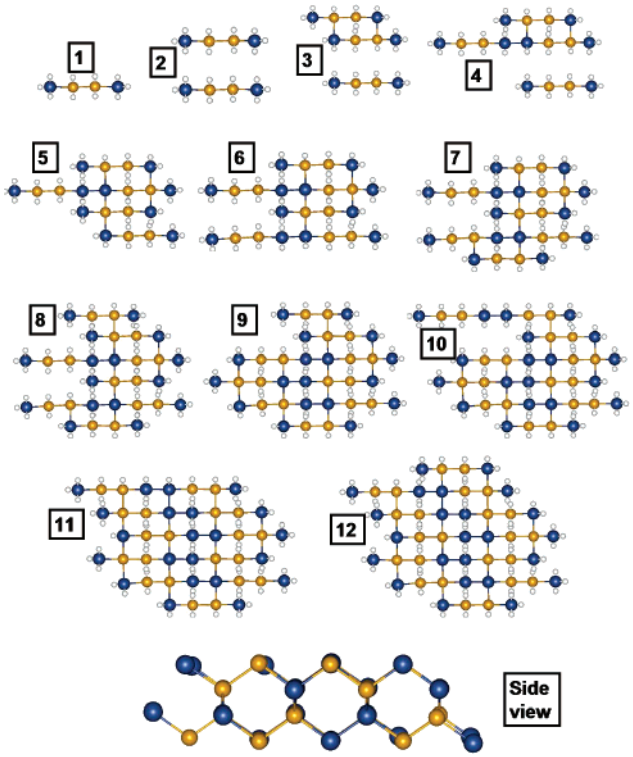

Figure 12. Hypothetical growth sequence of two-dimensional clusters of composition $Si_{0.50}Ge_{0.50}$ containing a random distribution of Si and Ge atoms. The schematic process illustrated (viewed along the normal to the (001) growth plane) involves the systematic condensation of GeSiSiGe molecules via elimination of H2. Legend: blue spheres, Ge; yellow spheres, Si; small white circles, H.

Experimental Section

All manipulations were carried out under inert conditions using standard Schlenk and drybox techniques. Dry, air-free solvents were distilled from either anhydrous $CaCl_2$ or sodium benzophenone ketyl

prior to use. All NMR spectra were collected either on a Varian INOVA 400 spectrometer operating at 400 MHz or a Gemini 300 spectrometer. Samples were dissolved in $CDCl_3$ or C_6D_6, and all nuclei were referenced either directly or indirectly to the proton signal of TMS or the residual solvent peak as indicated. IR spectra were recorded using a 10 cm gas cell with KBr windows. Elemental analyses were performed by Desert Analytics (Tucson, Arizona). Gas chromatography mass spectrometry (GCMS) data were obtained using a JEOL JMS-GC Mate II spectrometer. Powdered lithium (Aldrich), lithium tetrahydroaluminate (Aldrich), trichloro(*p*-tolyl)silane (Gelest), trifluoromethane sulfonic acid (Alfa Aesar), nonafluorobutane-1-sulfonic acid (Aldrich), and electronic grade germane gas (Voltaix, Inc.) were used as received. The starting materials *p*-tolylsilane, chloro(*p*-tolyl)silane, 1,2-bis(*p*-tolyl)disilane, and 1,2-bis(trifluoromethylsulfonyloxy)disilane were prepared according to literature procedures,[10] and their purities were checked by NMR spectroscopy. Potassium germyl was synthesized in monoglyme using sodium−potassium (80% K) alloy. The coupling reactions using powdered lithium were performed in a helium environment rather that in an N_2 atmosphere to prevent formation of lithium nitride.

(*p*-Tolyl)$_2$(SiH$_2$)$_2$: A solution of monochloro(*p*-tolyl)silane (10.0 g, 63.8 mmol) in di-*n*-butyl ether (120 mL) and toluene (40 mL) is stirred with sodium pieces (1.68 g, 146.2 mmol) for 5 h at 125 °C. The mixture is filtered, and the filtrate is distilled to remove the solvents and other impurities. The remaining colorless liquid product (4.40 g) was examined by NMR to determine its identity and purity and was subsequently used without purification.

(C$_4$F$_9$SO$_3$)$_2$(SiH$_2$)$_2$: A sample of $C_4F_9SO_3H$ (7.9 g, 26.3 mmol) was added to a 15 mL solution of 1,2-(*p*-tolyl)disilane (3.18 g, 13.1 mmol) in toluene at −40 °C. A colorless precipitate was immediately formed at low temperatures. The reaction flask was warmed to 23 °C and stirred for 1−2 h. The colorless solid was filtered and dried in vacuo. Repeated concentration and cooling of the toluene filtrate at −20 °C yielded additional product. Yield = 7.9 g (95%). Mp = 68 °C. ^{1}H NMR (300 MHz, $CDCl_3$): δ 5.078 (s, $^1J_{SiH}$ = 272 Hz, Si−H$_2$, $^3J_{HH}$ = 3.6 Hz). ^{29}Si NMR (79.5 MHz, $CDCl_3$): δ −30.1. Anal. Calcd for $C_8F_{18}S_2O_6Si_2H_4$: C, 14.59; H, 0.61; F, 51.95. Found: C, 14.27; H, 0.87; F, 51.74.

(H$_3$Ge)$_2$(SiH$_2$)$_2$, Method A: A 20 mL solution of (C$_4$F$_9$SO$_3$)$_2$(SiH$_2$)$_2$ (4.67 g, 9.5 mmol) was added to a slurry of $KGeH_3$ (2.00 g, 20.9 mmol) in diethyl ether (15 mL), at −40 °C. The reaction was then warmed to −10 °C and stirred under nitrogen for 12 h after which it was heated at 35 °C for an additional 1 h. The volatiles were fractionally distilled several times through U-traps held at −20, −50, and −196 °C. The −50 °C trap retained pure $(H_3Ge)_2(SiH_2)_2$ (260 mg, 26% yield), while the −196 °C trap contained solvent and traces of GeH_4 and SiH_4. Vapor pressure: 7.0 Torr (23 °C). IR (gas, cm^{-1}): 2147 (s), 2073 (vs), 910 (w), 879 (w), 799 (s), 740 (vw), 682 (s), 651 (m), 442 (vw). ^{1}H NMR (400 MHz, C_6D_6, 7.15 ppm): δ 3.106 (t, J = 4.1 Hz, 6H, Ge−H$_3$), δ 3.290 (q, J = 3.9 Hz, 4H, Si−H$_2$). ^{29}Si NMR (79.5 MHz, C_6D_6): δ −105.0 (this value is close to that observed for $(H_3Ge)_2SiH_2$ at −102.45). GC−MS: *m*/*z* 210−196 ($Si_2Ge_2H_x^+$), 180−170 ($SiGe_2H_{8-x}^+$), 152−143 ($Ge_2H_{6-x}^+$), 140−126 ($Si_2GeH_{8-x}^+$), 107−98 ($H_3SiGeH_3^+$), 77−72 (GeH_4^+), 62−58 ($Si_2H_{6-x}^+$), 32−28 (SiH_4^+).

(H$_3$Ge)$_2$(SiH$_2$)$_2$, Method B: A sample of $(CF_3SO_3)_2(SiH_2)_2$ (3.39 g, 9.5 mmol) was added to a slurry of 2.40 g (20.9 mmol) of $KGeH_3$ in diethyl ether (30 mL) at −30 °C. The mixture was then warmed to 23 °C and stirred under nitrogen for 5 h. The volatiles were fractionally distilled, and the $(H_3Ge)_2(SiH_2)_2$ product in its pure form was collected in a −50 °C trap (0.250 g, ∼13% yield).

(SiH$_2$GeH$_2$)(GeH$_3$)$_2$: The compound is obtained as a byproduct in the synthesis of $(H_3Ge)_2(SiH_2)_2$ and was isolated by repeated distillation through **U**-traps under static vacuum maintained at −20 and −50 °C to collect $(GeH_3)_2(SiH_2GeH_2)$ and $(H_3Ge)_2(SiH_2)_2$, respectively. Vapor pressure: 1.0 Torr (22 °C). IR (gas, cm^{-1}): 2145 (m), 2073 (vs), 910 (w), 878 (w), 793 (vs), 723 (w), 679 (w), 615 (s), 443 (vw). ^{1}H NMR (400 MHz, C_6D_6, 7.15 ppm): δ 3.30 (sept, J = 3.9 Hz, 2H, Si−H$_2$), δ 3.23 (t, J = 4.6 Hz, 3H, Ge−H$_3$), δ 3.13 (t, J = 3.90 Hz, 3H, Ge−H$_3$), δ 3.03 (sept, J = 4.0 Hz, 2H, Ge−H$_2$). ^{29}Si NMR (79.5 MHz, C_6D_6): δ −98.2. GC−MS: *m*/*z* 256−240 ($SiGe_3H_{10-x}^+$), 230−212 ($SiGe_2H_{8-x}^+$), 184−169 ($SiGe_2H_{8-x}^+$), 154−141 ($Ge_2H_{6-x}^+$), 136−128 ($Si_2GeH_{8-x}^+$), 108−98 ($SiGeH_{6-x}^+$), 77−70 (GeH_{4-x}^+), 32−28 (SiH_4^+).

Acknowledgment. This work was supported by the NSF (DMR-0221993 and DMR-0303237) and Voltaix Corporation. We also acknowledge the use of computational resources provided by the Goldwater Materials Visualization Facility in the Center for Solid State Science at Arizona State University.

Supporting Information Available: Complete ref 11. This material is available free of charge via the Internet at http://pubs.acs.org.

JA060428J